Strategies for Harnessing High Rate and Cycle Performance from Graphite Electrodes in Potassium-ion Batteries

Shubham Kaushik[a], *Keigo Kubota*[a], *Jinkwang Hwang*[b], *Kazuhiko Matsumoto*[a,b,*], *Rika Hagiwara*[a,b]

[a]AIST-Kyoto University Chemical Energy Materials Open Innovation Laboratory (ChEM-OIL) Sakyo-ku, Kyoto 606-8501, Japan

[b]Graduate School of Energy Science, Kyoto University, Sakyo-ku, Kyoto 606-8501, Japan

*Corresponding Author E-mail Address: k-matsumoto@energy.kyoto-u.ac.jp

Keywords: Inorganic ionic liquid electrolyte, potassium ion batteries, intermediate temperature, graphite negative electrode, high rate capability

Abstract

Potassium-ion batteries (PIBs) have been lauded as the next-generation energy storage systems on account of their high voltage capabilities, low costs, and the high abundance of potassium resources. However, the practical utility of PIBs has been heavily encumbered by severe K metal dendrite formation, safety issues, and insufficient electrochemical performance during operations—indeed critical issues that underpin the need for functional electrolytes with high thermal stability, robust solid electrolyte interphase (SEI) forming capabilities and high electrochemical performance. In a bid to establish a knowledge framework for harnessing high rate capabilities and long cycle life from graphite negative electrodes, this study presents the physical properties and electrochemical behavior of a high K^+ concentration inorganic ionic liquid (IL) electrolyte, K[FSA]-Cs[FSA] (FSA^- = bis(fluorosulfonyl)amide) (54:46 in mol), at intermediate temperatures of 70 °C. This IL electrolyte demonstrates an ionic conductivity of 2.54 mS cm^{-1} and a wide electrochemical window of 5.82 V. Charge-discharge tests performed on a graphite negative electrode manifest a high discharge capacity of 278 mAh g^{-1} (0.5C) at 70 °C, a high rate capability (106 mAh g^{-1} at 100C), and a long cycleability (98.7% after 450 cycles). Stable interfacial properties observed by electrochemical impedance spectroscopy during cycling are attributed to the formation of sulfide-rich all-inorganic SEI, which was examined through X-ray photoelectron spectroscopy. The performance of the IL is collated with that of a *N*-methyl-*N*-propylpyrrolidinium based organic IL to provide insight into the synergism between the highly concentrated K^+ electrolyte at intermediate temperatures and the all-inorganic solid-electrolyte interphase during electrochemical operations of the graphite negative electrode.

1. Introduction

Anchoring innumerable applications—among others, portable electronic devices and electric vehicles—lithium-ion batteries (LIBs) have become the quintessential rechargeable batteries due to their unmatched energy densities and long cycle life.[1-2] Despite this success, concerns over the rapidly depleting lithium resources and the high costs associated with LIB development continue to cast doubts over the future of these energy storage systems. As such, contemporary research efforts have shifted towards alternative energy chemistries such as Na-ion, Mg-ion, K-ion, and Al-ion systems in the pursuit of environmentally benign materials with high theoretical energy densities.[3-4]

Amongst the LIB alternatives fielded so far, potassium-ion batteries (PIBs) have emerged as providential contenders due to the terrestrial abundance (global potash reserves: 7000 million tons *vs.* global Li_2CO_3 reserves: 21 million tons) and low costs (potash prices: 830 USD ton^{-1} *vs.* Li_2CO_3 prices: 8000 USD ton^{-1}) of K resources.[5] Besides these advantages, K presents other ancillary chemical properties that inspire inquests into PIBs. For instance, K^+/K exhibits a lower redox potential (−2.93 V vs. SHE) than Li^+/Li (−3.04 V vs. SHE),[6-7] auguring the possibilities of high voltage and consequently high energy densities. Additionally, PIBs can be expected to deliver high power densities due to the excellent K^+ diffusion proffered by its small Stokes radius (*e.g.*, 3.6 Å for K^+ compared to 4.8 Å for Li^+ in propylene carbonate), in conjunction with the lower desolvation energy of K^+ provided by its weak Lewis acidity.[8-9] These electrochemical advantages are further complimented by the low reactivity between K and Al which enables the utilization of cheaper Al current collector at the negative electrode side instead of the costly Cu current collectors presently used in LIBs. Owing to these merits, PIBs have been highly explored as promising candidates for battery systems.[10-13] Even so, the advancement of PIBs is heavily

encumbered by severe K metal dendrite formation, poor solid-state K-ion diffusion, and high flammability of organic solvents—indeed critical issues that highlight the need for functional electrolytes for PIB operations.

As with other battery systems, electrolyte choice is an essential aspect of PIB development as it determines critical operational parameters such as electrochemical performance (reversible capacity, initial Coulombic efficiency, rate capability, and cycleability), the solid electrolyte interface (SEI) formation, and safety. Due to the similarities in K and Li electrochemistry (both group 1A elements), K-analogues of well-established LIB electrolytes such as lithium hexafluorophosphate (Li[PF_6]) salt dissolved in ethylene carbonate (EC) and diethyl carbonate (DEC) have gained utility among PIBs due to their ability to form thermodynamically stable K graphite intercalated compounds (KGICs). Carbonaceous materials have shown considerable promise as negative electrode materials for PIBs.[14-15] In fact, a previous study investigating the electrochemical K^+ intercalation behavior of graphite negative electrodes in a 0.8 mol dm^{-3} K[PF_6]-EC:DEC (1:1 v/v) electrolyte reported a remarkably high reversible capacity of 273 mAh g^{-1} (comparable to the theoretical capacity of 279 mAh g^{-1}) at the current density of C/40 (1C = 279 mA g^{-1}).[16] The resulting reversible capacity of 273 mAh g^{-1} is close to the theoretical capacity of 279 mAh g^{-1}. However, the electrolyte portrayed poor efficacy marked by a low initial Coulombic efficiency of 57.4% an inferior capacity retention of 50.8% after 50 cycles, deeming it unsuitable for practical applications. In a bid to establish the factors influencing PIB performance, another study comparatively analyzed the electrochemical performance of a 3 mol dm^{-3} K[FSA] (FSA^- = bis(fluorosulfonyl)imide) in dimethyl ether (DME) electrolyte against that of the 0.8 mol dm^{-3} K[PF_6]-EC:EMC (1:1 v/v) electrolyte with the aid of O-doped carbon negative electrodes. Here, the 3 mol dm^{-3} K[FSA]-DME electrolyte was reported to achieve an initial Coulombic

efficiency of 58.5% with an improved capacity retention of 91.5% after 3000 cycles: notably, superior performance compared to that of the 0.8 dm^{-3} $K[PF_6]$-EC:EMC which delivered an initial Coulombic efficiency of 49.8% and capacity retention of 48.5% after 430 cycles.[17] Through X-ray photoelectron spectroscopy (XPS) and transmission electron microscopy (TEM), the study further attributed the remarkable performance improvement observed in the 3 mol dm^{-3} K[FSA]-DME electrolyte to the formation of a robust solid electrolyte interphase (SEI) layer which mainly consisted of inorganic components. On the other hand, the 0.8 dm^{-3} $K[PF_6]$-EC:EMC system was noted to facilitate the formation of an inhomogeneous organic/inorganic SEI layer with poor electronic properties. The beneficial properties of the $[FSA]^-$ anion were further confirmed by a subsequent probe into the performance of a $K[PF_6]$/K[FSA]-EC:DEC binary salt electrolyte.[18] In this study, a K/graphite system comprising a binary salt electrolyte (in the ratio of 0.75$K[PF_6]$/0.25K[FSA]) attained an initial Coulombic efficiency of 89%, which was higher than that of the electrolyte entirely based on the $K[PF_6]$ system (80%). Further, a graphite/$K_2Mn[Fe(CN)_6]$ full cell with the 0.75$K[PF_6]$/0.25K[FSA]-EC:DEC binary electrolyte system achieved better capacity retention over 500 cycles than the $K[PF_6]$-EC:DEC electrolyte. In addition, the K[FSA] salt has been found to have high solubility in ether or ester solvents[19] as well as dendrite suppression capabilities in half-cell configurations—properties poised to facilitate high performances.[20-21] These properties were exemplified by a highly concentrated 7 mol kg^{-1} K[FSA]-DME electrolyte wherein a high plating/stripping efficiency of K metal, suppression in Al corrosion at high voltage, and excellent capacity retention were observed in K/graphite and K/$K_2Mn[Fe(CN)_6]$ half-cell operations.[19] However, it is worth noting that even though the $[FSA]^-$ anion has been shown to facilitate the formation of uniform and robust SEI layer, the presence of

organic solvent(s), even in small amounts, induces a large interfacial resistance[22] on the K counter/reference electrode(s) thereby compromising the practicality of the battery.

The detrimental effects of organic solvents on battery performance have sparked interest in ionic liquids (ILs) as alternative electrolytes for a variety of battery systems (LIBs,[23] Na-ion batteries (SIBs)[24], Li-S batteries[25], and Na-S batteries[26]). This class of electrolytes has been endowed with a trove of exquisite physicochemical properties such as negligible flammability, low volatility, high thermal stability, and wide electrochemical window that facilitate safe operations in a wide temperature range.[27-29] In addition, several studies have reported remarkable improvements in rate capabilities and cycle life during operations at intermediate temperatures[30-31], thus presenting unique technical and economical prospects of reclaiming ubiquitous waste heat from everyday operations.[32-33] Furthermore, several studies have attributed the superior performances observed in ILs to the formation of uniform and robust SEI layers during electrochemical operations.[34-35] Among LIBs, a Li[FSA]-[C_2C_1im][FSA] (C_2C_1im = 1-ethyl-3-methylimidazolium) IL electrolyte was found to have excellent Li metal dendrite suppression capabilities at 25 °C, demonstrating a stable Li deposition/dissolution marked by a consistent overpotential of 12 mV for 1000 h (2500 cycles) at 1 mA cm^{-2}.[36] In contrast, a Li[PF_6]-EC:DMC organic electrolyte under the same conditions manifested a significant increase in overpotential after 246 h (615 cycles). Likewise, in SIBs, a Na/mesoporous-carbon system using a high concentration 3.8 mol dm^{-3} Na[FSA]-[C_3C_1pyrr][FSA] (C_3C_1pyrr = *N*-methyl-*N*-propylpyrrolidinium) IL electrolyte was recently reported to attain a superior rate capability and cycle life than a 1 mol dm^{-3} Na[FSA]-EC:DMC under similar conditions.[37] Temperature-dependent electrochemical impedance spectroscopy (EIS) combined with XPS performed in the study further confirmed the superior performance of the IL to emanate from its intrinsically fast

Na^+ diffusion capabilities coupled with the presence of a robust SEI composed of inorganic components. On the other hand, the analyses accredited the inferior performance of the Na[FSA]-EC:DMC electrolyte to the formation of a thick SEI mainly consisting of organic species.

Although IL electrolytes have displayed outstanding performance among LIBs and SIBs, their exploration in PIBs is relatively limited, with inquests primarily focusing on $[FSA]^-$ and $[TFSA]^-$ (TFSA = bis(trifluoromethanesulfonyl)imide) anions. Even so, ILs based on potassium have displayed promising physicochemical properties that point towards favorable performance in PIBs. For instance, the K[FSA]-[C_3C_1pyrr][FSA] (20:80 in mol) IL was reported to entail a higher ionic conductivity of 4.8 mS cm^{-1} and a wider electrochemical window of 5.72 V at 25 °C—significantly higher than its Li (3.6 mS cm^{-1} and 5.48 V) and Na (3.6 mS cm^{-1} and 5.42V) counterparts at the same temperatures.[38] Other works have also reported the 0.5 mol dm^{-3} K[TFSA]-[C_3C_1pyrr][TFSA] IL electrolyte to have good compatibility with high voltage positive electrode materials of $K_2Ni_2TeO_6$ and $K_{2/3}Ni_{1/3}Co_{1/3}Te_{1/3}O_2$, delivering stable electrochemical performance in a wider electrochemical window of 6.01 V than that of the $[FSA]^-$ system.[39-40] Similarly, the IL electrolytes have been noted to deliver superior electrochemical performance with a variety of negative electrode materials such as hard carbon,[41] Sn,[42] Sn_4P_3 [43], and graphite negative electrode materials. In a study focusing on the electrochemical performance of a commercially ball-milled graphite negative electrode material, the K[FSA]-[C_3C_1pyrr][FSA] IL (20:80 in mol) electrolyte was reported to attain exceptional capacity retention of over 99% after 400 cycles as well as a high rate capability exemplified by a capacity retention of 88% at 2C (referenced against the capacity at C/20).[44] The cycle performance of a graphite negative electrode in the 1 mol dm^{-3} K[FSA]-[C_3C_1pyrr][FSA] IL (94.7% after 1000 cycles) has also been reported to be higher than in the K[FSA]-EC:DEC organic electrolyte.[45] Surface analysis conducted in this

study using XPS attributed the enhanced performance observed in the IL electrolyte to the formation of a robust SEI layer composed of decomposition products from $[C_3C_1pyrr]^+$ and $[FSA]^-$.

Explorations into different IL electrolyte systems further revealed single K^+ cation inorganic ILs such as the K[FSA]-K[FTA] (FTA = (fluorosulfonyl)-(trifluorosulfonyl)amide) electrolyte to manifest high ionic conductivities and wide electrochemical windows.[46] However, a K/graphite half-cell employing the K[FSA]-K[FTA] IL electrolyte at 80 °C was only able to achieve a low initial Coulombic efficiency of 42.7% and low capacity retention of 84.2% after 50 cycles. A summary of the electrochemical performance of graphite-based negative electrode materials in a variety of organic and IL electrolytes for PIBs has been furnished in **Table 1**.

Looking into the previous reports presented in this section, the exceptional performance of K[FSA]-[C_3C_1pyrr][FSA] (20:80), even in comparison to other IL electrolytes, can be attributed to the formation of stable SEI derived from $[FSA]^-$. Although several studies have suggested the use of highly concentrated electrolytes incorporating K[FSA] to improve the interfacial properties of organic electrolytes[20,47], the drastic increase of the liquidus line (82 °C at 30 mol% K[FSA]) of the K[FSA]-[C_3C_1pyrr][FSA] IL does not allow this system to be used at higher concentrations at room temperature conditions (25 mol% of K[FSA] corresponding to 1.26 mol dm^{-3}). A careful literature survey brought to our attention the K[FSA]-Cs[FSA] inorganic IL with a eutectic point of 63 °C at 54:46 in mol ([K,Cs][FSA] IL hereafter) as a high K-salt concentration IL system.[48] Although this electrolyte has not been explored for PIBs, it is posited to engender high electrochemical performance in intermediate-temperature operations and at high K^+ concentrations. Additionally, operation at intermediate temperatures is expected to improve the electrolyte's K metal dendrite suppression capabilities, ionic conductivities, and the wettability of the IL electrolyte—recipes for even better performance.

In a bid to elucidate the factors influencing the performance of graphite negative electrodes in high K-salt concentration IL systems for PIBs, this study presents a comprehensive analysis of the physicochemical properties, electrochemical behavior, and intercalation mechanisms of the inorganic [K,Cs][FSA] IL electrolyte in comparison with a previously reported K[FSA]-[C_3C_1pyrr][FSA] IL (20:80 in mol) (hereafter, [K,C_3C_1pyrr][FSA] IL). The physicochemical properties and electrochemical performance of the [K,Cs][FSA] IL electrolyte are evaluated at 70 °C (intermediate temperature)—a temperature slightly above the eutectic point of the [K,Cs][FSA] IL (63 °C) and the melting point of K metal (64 °C). Through a series of controlled analyses using cyclic voltammetry, galvanostatic charge-discharge tests, rate capability analyses, cycle performance analyses, and X-ray photoelectron spectroscopy (XPS) performed on half-cell and symmetric cell configurations, we clearly establish the effects of ionic species on electrochemical performance.

2. Experimental

General procedure. All the moisture- and air-sensitive materials were handled and prepared in a glove box (Miwa Manufacturing Co., Ltd.) filled with dry Ar gas (H_2O < 1 ppm and O_2 < 1 ppm). The salts, K[FSA] (TCI chemicals, purity >95%), and [C_3C_1pyrr][FSA] (Kanto Chemical, purity >99.9%) were dried under vacuum overnight at 80 °C.

Synthesis and characterization of Cs[FSA]. The Cs[FSA] powder was prepared via an ion-exchange method prescibed in a previous study.[49] The resulting Cs[FSA] adopts the Form I structure within two known polymorphs according to the vibrational spectroscopic data (see below).[50] Combustion analysis (Calc): N, 4.5; F, 12.1%. (Found) N, 4.5; F, 12.1%. Raman: $\tilde{\nu}$ [cm^{-1}]

(Intensity) = 1365 (59), 1216 (97), 1174 (60), 842 (59), 728 (100), 575 (70), 564 (63), 525 (61), 484 (62), 457 (73), 358 (77), 327 (66), 291 (76), 157 (59). IR (ATR): $\tilde{\nu}$ [cm^{-1}] = 1374 (m), 1352 (m), 1220 (sh), 1176 (s), 1115 (m), 831 (m), 735 (s), 721 (s), 643 (vw), 562 (vs), 482 (vw), 453 (w), 433 (vs: very strong, s: strong, m: middle, w: weak, and vw: very weak, sh: shoulder). See **Figure S1a** and **1b** for the corresponding Raman and IR spectra. Detailed assignment have been furnished in a previous report.[50]

Preparation of IL electrolytes: The [K,Cs][FSA] IL electrolyte (K[FSA]-Cs[FSA] = 54 : 46 in mol) was prepared by hand-grinding the corresponding precursor salts. The [K,C_3C_1pyrr][FSA] IL (K[FSA]-[C_3C_1pyrr][FSA] = 20 : 80 in mol) was prepared by stirring K[FSA] and [C_3C_1pyrr][FSA] overnight at 25 °C.

Physiochemical characterization:

Raman spectra were recorded by a DXR3 Smart Raman spectrometer (Thermo Fisher Scientific) using a 532 nm diode-pumped solid-state laser. The sample used for Raman spectroscopy was sealed in a glass cell and isolated from air. Fourier-transformed IR spectra were recorded by an IR spectrometer (ALPHA II, Bruker Optics Laboratories, Inc.) equipped with an attenuated total reflection (ATR) module under a dry air atmosphere. The viscosity of the [K,Cs][FSA] IL was measured using an electro-magnetically spinning viscometer (Kyoto Electronics Manufacturing Co., Ltd., EMS100) in the temperature range of 130–60 °C at intervals of 10 °C. The [K,Cs][FSA] powder was sealed in a glass tube with a spherical Al probe inside the glove box, followed by heating up to 130 °C. An electrochemical analyzer (HOKUTO DENKO, HZ-Pro) was used to measure the specific conductivities of the samples through AC impedance spectroscopy at an AC

perturbation of 10 mV. The sample was sealed in a cell with two Pt black electrodes (RADIOMETER ANALYTICAL). The cell of which the cell constant was obtained by measuring the conductivity of the KCl-saturated standard solution was placed in the dry chamber for measurement.

Electrode preparation and battery assembly: All the electrochemical tests were performed using a 2032-type coin-cell at 25 and 70 °C. To prepare the working electrodes, natural graphite powder samples (with a mean particle diameter of 3 and 10 μm) were each mixed with polyamideimide binder in the ratio of 80:20 w/w and *N*-methyl-2-pyrrolidone solvent. The resulting slurry was cast onto an Al foil and dried under vacuum at 60 °C. Subsequently, 10 mm φ disc electrodes were punched and dried under vacuum at 120 °C. The average mass loading of the active material was 1.5 mg cm^{-2} after the drying process. Metallic K (Sigma-Aldrich, >99.5% purity) discs pressed on Al current collectors (16 mm φ discs) were used as counter electrodes. The end of separator on potassium metal side (20 mm φ) was folded to confine the molten potassium metal for the measurement at 70 °C. A glass fiber filter (Whatman, GF-A, 260 mm in thickness and 20 mm in diameter) soaked with the electrolyte was used as a separator. Prior to the coin cell assembly, the electrolyte powder was vacuum-impregnated into the graphite working electrode and separator at 120 °C to remove Ar gas in the pores. The amount of electrolyte per coin-cell was maintained at 500 mg.

Electrochemical measurement: The assembled cells were charged and discharged using an HJ1001SD8 test device (Hokuto Denko, Japan). The operation temperature was controlled at 70 °C with the ESPEC SU221 thermostatic chamber and the coin-cells were kept at the open-circuit

voltage for 3 h before testing. The charging and discharge processes were controlled by a constant-current constant-voltage and constant-current modes. After charging the cells at a constant current of 0.01 V, a constant voltage was maintained at 0.01 V until the current reached 10% of the value of the constant current step. Cyclic voltammetry (CV), K metal deposition/dissolution tests, and EIS were performed using a VSP potentiostat (Bio-Logic). The electrochemical window of the [K,Cs][FSA] IL electrolyte was determined by CV at a scan rate of 5 mV s^{-1} at 70 °C using Al and Pt plate working electrodes (8 mm in diameter). The K/K symmetric cell was constructed using a 2032-type coin cell consisting of the IL electrolyte and two separators. Two Kapton films (outer diameter = 16 mm and inner diameter = 6 mm) were placed around the K metal electrode to precisely control the electrode area. The K metal deposition/dissolution test was conducted at 1 mA cm^{-2} with 5 min-deposition and 5 min-dissolution). The EIS measurements for graphite/graphite symmetric cells were carried over a frequency range of 100 kHz – 10 mHz at an amplitude of 20 mV. Prior to the symmetric cell assembly, the graphite electrodes were charged to a 50% state of charge using a half-cell configuration comprising the respective electrolytes. The symmetric cells were assembled using two graphite electrodes with identical mass loading.

Post characterizations: The graphite working electrodes cycled in K/graphite half-cells were washed with tetrahydrofuran (Wako Pure Chemical Industries, Japan, water content < 10 ppm) and dried under vacuum overnight prior to XPS (JPS-9010, JEOL Ltd.) and ex-situ X-ray diffraction (XRD, Smart lab, Rigaku Corp.) analyses. The XPS samples were analyzed after the 2nd charge-discharge cycle with MgKα at 10 kV–10 mA. The sample subjected to XPS was transferred from the glove box to the instrument using an air-tight cell to avoid exposure to the air. To investigate the SEI layer components, Ar ion etching was performed for 1 min at ionization

energy of 400 eV. The XRD patterns of the charged and discharged samples were obtained using an XRD diffractometer with the CuKα line (λ =1.5418 Å) at 40 kV–30 mA.

3. Results and discussion

As previously highlighted (see Introduction section), ionic liquids are endowed with wide electrochemical windows that facilitate elevated temperature operations but also confer the possibilities of improved performances. Therefore, in order to ascertain the influence of temperature on the physicochemical and electrochemical properties of the present [K,Cs][FSA] IL electrolyte, viscosity and ionic conductivity measurements were obtained in the 60–130 °C temperature range (see **Table S1** for detailed values). **Figure 1** summarizes the physical and electrochemical properties of the [K,Cs][FSA] IL electrolyte. The results were fitted using the VTF (Vogel−Tammann−Fulcher) equation shown below;[51]

$$\eta = A_\eta \sqrt{T} \exp\left(\frac{B_\eta}{T - T_\eta}\right) \qquad (1)$$

$$\sigma = \frac{A_\sigma}{\sqrt{T}} \exp\left(-\frac{B_\sigma}{T - T_\sigma}\right) \qquad (2)$$

Here, η, σ, and T represents the viscosity, ionic conductivity, and absolute temperature of the electrolyte, respectively. The A_η, A_σ, B_η, B_σ, $T_{0\eta}$, and $T_{0\sigma}$ are the mathematical fitting parameters. The values of viscosities and ionic conductivities were found to be in good accord with Equations (1) and (2) (R^2 > 0.999) (see **Table S2** for fitting parameters). The resulting VTF plots show a convex curve for the temperature dependence of IL viscosity (**Figure 1a**) and a concave curve for

the temperature dependence of ionic conductivity (**Figure 1b**)—in agreement with previously reported IL behavior.[52-53] The viscosity of the [K,Cs][FSA] IL, which was moderate (in the order of 10 mPa s) in the 100–130 °C temperature range, was observed to significantly increase to the order of 10^2 mPa s in the 60–90 °C temperature range. Nonetheless, the viscosity ((279 mPa s) and ionic conductivity (2.54 mS cm^{-1}) of the [K,Cs][FSA] electrolyte at 70 °C were noted to be intermediate values falling between the previously reported values of the [K,C_3C_1pyrr][FSA] organic IL (19.4 mPa s and 16.7 mS cm^{-1}) and the $K[FSA]_{0.55}[FTA]_{0.45}$ IL (1807.9 mPa s and 1.05 mS cm^{-1}) electrolytes at the same temperature.[38, 46]

In order to measure the electrochemical window of the [K,Cs][FSA] IL electrolyte, cyclic voltammetry was performed at 70 °C. The cathodic and anodic scans were performed using two-electrode coin cells comprising K metal counter electrode alongside Al or Pt metal working electrodes, respectively. The combined cyclic voltammograms for the negative and positive potential regions are shown in **Figure 1c**. In the negative potential region, a K metal deposition-dissolution process was observed at 0 V vs. K^+/K with a Coulombic efficiency of 75.5%. The anodic limit of 5.82 V vs. K^+/K was determined at the potential where the current density reaches 0.2 mA cm^{-2} which corresponds to the oxidation of $[FSA]^-$. The electrochemical window and first-cycle Coulombic efficiency of this IL electrolyte is noticeably higher than those reported from the [K,C_3C_1pyrr][FSA] (5.72 V and 72.7%) organic and $K[FSA]_{0.55}[FTA]_{0.45}$ inorganic IL electrolytes (5.60 V and 60%).[38, 46] As shown in **Figure 1d**, the overpotential during the K deposition/dissolution process in the K/K symmetric cell increased from 140 mV to 270 mV in the first 10 h, after which it was noted to gradually decrease to 140 mV after 100 h: indicating the long term stability of the K metal counter electrode in the [K,Cs][FSA] IL electrolyte at 70 °C.

Electrochemical performance of a graphite negative electrode material was investigated with two different IL electrolyte systems: [K,Cs][FSA] and [K,C_3C_1pyrr][FSA] to compare the effects of ionic species on its electrochemical behavior. According to a previous work, the performance of the graphite negative electrodes in PIBs can be influenced by the size of the constituent graphite particles. Here, ball-milled graphite was found to yield higher reversible capacities and cycleability than the pristine graphite,[54] as a result of the mechanical exfoliation of graphene layers, defect formation, and reduction of particle size. However, for practical applications, large-sized graphite particles are preferred due to their higher tap densities and lower initial irreversible capacities. Thus, prior to the comparative analyses using the two ILs, a preliminary investigation on the charge-discharge behavior of two different-sized graphite (3 and 10 μm) was conducted using K/graphite half-cells containing the [K,C_3C_1pyrr][FSA] IL electrolyte at 25 °C and 70 °C (see **Figure S2** and additional comments for details). Although both electrodes (the 3 μm and the 10 μm graphite) delivered comparable discharge capacities (281 and 278 mAh g^{-1} for the 3- and 10-μm, respectively) during the initial cycle, the 10 μm graphite exhibited a higher initial Coulombic efficiency (67.5%) than the 3 μm graphite electrode (44.2%) at 70 °C. Therefore, the 10 μm graphite was selected as the electrode of choice for further investigations at 70 °C.

The graphite (10 μm) negative electrodes were subjected to galvanostatic charge-discharge tests using K/graphite half-cells comprising the [K,Cs][FSA] (**Figures 2a** and **2c**) and [K,C_3C_1pyrr][FSA] IL electrolytes (**Figures 2b** and **2d**) at 70 °C at the current rate of 0.5C (additional constant voltage at 0.01 V during charge). As illustrated by the charge-discharge curves (from the three initial cycles), the initial cycle of both the [K,Cs][FSA] and the [K,C_3C_1pyrr][FSA] IL electrolytes delivered remarkable discharge capacities of 278 and 279 mAh g^{-1} (theoretical capacity = 279 mAh g^{-1} for KC_8 formation), with initial Coulombic efficiencies of 66.0 and 67.5%,

respectively. The second and third cycles yielded superposing charge-discharge curves with Coulombic efficiencies exceeding 95%, evincing the high reversibility of the intercalation/deintercalation processes into/from graphite electrodes in both electrolytes.

Further, the d*Q*/d*V* plots from both electrolytes (**Figure 2c** and **2d**) manifest the occurrence of similar four-step K^+ intercalation/deintercalation mechanism(s) in both cases, *albeit* with marginally lower polarization in the [K,Cs][FSA] IL electrolyte. The redox peak voltages observed here correspond with the sequential formation of KC_{48} (stage-4), KC_{36} (stage-3), KC_{16} (stage-2), and KC_8 (stage-1) K-graphite intercalation compounds (K-GICs), as has been reported in previous studies.[44]

The K^+ intercalation/deintercalation mechanism(s) fostered by the [K,Cs][FSA] IL electrolyte were further examined by performing *ex-situ* X-ray diffraction (XRD) measurements on the graphite negative electrode after full-charge to 0.01 V and full-discharge to 2.0 V at a current density of 0.5C. As visualized in **Figure S3**, the XRD pattern of the electrode after full-charge is characterized by the 001 and 002 diffraction peaks appearing at 16.57° (d = 5.350 Å) and 33.55° (d = 2.671 Å), respectively—which confirms that the fully potassiated KC_8 phase had been formed.[55-56] It is worth mentioning that the electrode also displayed two unknown peaks appearing at 28.52° and 30.58°, in congruence with an observation from a previous report.[57] Although no detailed discussion on these peaks has been availed in previous literature, their intensities were noted to increase with prolonged exposure to air, suggesting that they originate from undesired reactions between the highly reactive KC_8 K-GICs and air before or during XRD measurements. Upon discharge to 2.0 V, the sharp 002 characteristic peaks for graphite are formed again, demonstrating that electrolyte was able to facilitate complete depotassiation with high reversibility.

The rate capabilities of the graphite negative electrode with the [K,Cs][FSA] IL and [K,C_3C_1pyrr][FSA] IL electrolytes were further investigated at 70 °C, as illustrated by **Figure 3a**. The current densities for both the charge and discharge processes were sequentially raised from 0.5C to 100C (additional constant voltage at 0.01 V during charging), whereafter cycling was conducted at 20C (5 cycles per rate). The [K,Cs][FSA] IL electrolyte exhibited remarkably high capacity retentions of 270, 266, 258, 250, 239, 204, and 106 mAh g^{-1} at 1, 2, 5, 10, 20, 50, and 100C, respectively (see **Figure S4a** for corresponding charge-discharge curves). The [K,C_3C_1pyrr][FSA] IL electrolyte yielded similar capacity retentions up to 10C (273, 268, 265, and 247 mAh g^{-1} at 1, 2, 5, and 10, respectively), after which a significant drop in the discharge capacity was observed at the higher current densities of 20C (226 mAh g^{-1}), 50 C (104 mAh g^{-1}), and 100 C (38 mAh g^{-1}) (see **Figure S4b** for corresponding charge-discharge curves). The rate capability results also revealed another key difference in the cell recuperation behavior of the two IL electrolytes. When the current rate was changed from 100 C to 20 C (from 40th to 41st cycle), the capacity of the cell with the [K,Cs][FSA] IL electrolyte reverted to 223 mAh g^{-1}. However, the [K,C_3C_1pyrr][FSA] IL electrolyte manifested a significantly lower capacity of 175 mAh g^{-1}, evincing that an irreversible deterioration reaction involving the organic cation had occurred. Comparing the charge-discharge curves obtained from the two IL electrolytes during the rate capability tests (**Figure S4**), the polarization in the [K,Cs][FSA] IL is seen to be lower than in the [K,C_3C_1pyrr][FSA] IL electrolyte in both charge and discharge processes—further ratification that the K,Cs][FSA] IL electrolyte entails superior electrode kinetics than the [K,Cs][FSA] IL.

For a clear picture into the K^+ kinetic behavior in the graphite negative electrode, EIS measurements of graphite/graphite symmetric cells containing the [K,Cs][FSA] and [K,C_3C_1pyrr][FSA] IL electrolytes at 70 °C were obtained after 1st, 10th, and 20th cycles. Prior to

the symmetric cell assembly, the graphite electrodes were charged to a 50% state of charge (SOC) using K/graphite half-cells with the respective electrolytes. Nyquist plots obtained from the operations with both IL electrolytes illustrate compressed semicircles, as shown in **Figures 3b** and **3c**. The Nyquist plots were fitted according to the equivalent circuit given in **Figure 3d**. Here, R_1 represents the bulk resistance, R_2 denotes the SEI-layer resistance (characteristic frequency = 500–3000 Hz), and R_3 corresponds to the interfacial resistances (characteristic frequency = 1–100 Hz), Q_2 and Q_3 show the corresponding constant phase element (CPE) for R_2 and R_3, respectively (see fitting parameters in Table S3). The R_1 values of the [K,Cs][FSA] IL electrolyte are noted to be significantly higher than those of the [K,C_3C_1pyrr][FSA] IL electrolyte, in congruence with the inherently lower ionic conductivity observed earlier in [K,Cs][FSA] IL electrolyte (**Figure 1**). However, the R_3 values recorded from the [K,Cs][FSA] IL electrolyte (65.6, 48.5, and 55.9 ohms after 1st, 10th, and 20th cycles, respectively) were significantly lower than those in the [K,C_3C_1pyrr][FSA] IL electrolyte (135.1, 122.1, and 134.9 ohms after 1st, 10th, and 20th cycles, respectively). The results here suggest that the high rate capabilities visualized in the [K,Cs][FSA] inorganic IL electrolyte were as a result of lower interfacial resistances.

The long-term performance of the graphite electrode during operations in the [K,Cs][FSA] IL electrolyte and the [K,C_3C_1pyrr][FSA] IL electrolytes at 70 °C was investigated through cycle performance tests (450 cycles) on the K/graphite half-cells at the current rate of 20C (**Figure 4a**). Here, the graphite negative electrode in the [K,Cs][FSA] IL electrolyte shows stable capacity and Coulombic efficiency throughout the cycles, delivering a discharge capacity of 210 mAh g^{-1} and a Coulombic efficiency of 98.7% at the 450th cycle. On the other hand, the [K,C_3C_1pyrr][FSA] IL electrolyte displays a gradual decrease in capacity up to the 150th cycle, whereafter fluctuations in both capacity and Coulombic efficiency are observed in the discharge capacity, evidencing the

intrinsic instability of this system which is accompanied by a rapidly increasing Coulombic efficiency (178% at the 450th cycle). **Figures 4b** and **4c** show the charge-discharge curves obtained during cycling with the two IL electrolytes. The [K,Cs][FSA] IL electrolyte (**Figure 4b**) displayed superposing charge-discharge curves characterized by long plateaus around the 0.5 V region during discharge. However, cycling in the [K,C_3C_1pyrr][FSA] IL electrolyte (**Figure 4c**) was noted to result in increasing polarization, further corroborating the deteriorating performance previously observed.

Previous studies on ILs have shown SEI layers containing inorganic components tend to facilitate high performances in LIBs[58-59] and SIBs,[37, 60] alike. In a bid to ascertain the nature of SEI layers formed by the [K,Cs][FSA] and [K,C_3C_1pyrr][FSA] IL electrolytes, X-ray photoelectron spectroscopy (XPS) measurements of the graphite electrodes were taken after the first cycle. **Figure 5** shows XPS spectra of the graphite electrodes in the N 1s (**Figure 5a** and **d**), S 2p **(Figure 5b** and **e**), and F 1s (**Figure 5c** and **f**) regions before and after one minute of Ar-ion etching. The deconvoluted N 1s spectra obtained before Ar-ion etching the graphite electrode from the [K,Cs][FSA] IL electrolyte show peaks corresponding to C–N (402.2 eV), N–SO^- (400.7 eV), and –N=SO (399.2 eV) bonds which can be attributed to the decomposition product of $[FSA]^-$ anions (**Figure 5a)**. Although the source of the C–N bond cannot be clearly determined at this stage, it appears to be a product of a reaction between graphite and the decomposition products of $[FSA]^-$. Spectra obtained after Ar-ion etching shows the peak intensity of the C–N bond to diminish while that of the –N=SO (399.2 eV) bond is noted to increase considerably.

In the case of N 1s spectra obtained before Ar-ion etching the graphite electrodes cycled in the [K,C_3C_1pyrr][FSA] IL electrolyte (**Figure 5d**), similar peaks ascribed to the $[FSA]^-$ decomposition products were visualized *albeit* alongside additional peaks related to the C–N^+

(403.5 eV) bond caused by the decomposition of $[C_3C_1pyrr]^+$. This observation is consistent with previous reports on the electrolyte.[36-37, 45] Upon Ar-ion etching, the peaks intensities of the –N=SO bonds are noted to increase dramatically while those of the $C–N^+$-related bonds are to become weaker. This observation suggests that the decomposition products of the $[FSA]^-$ were covered with the $[C_3C_1pyrr]^+$ decomposition products, suggesting that $[FSA]^-$ decomposes at higher potentials than $[C_3C_1pyrr]^+$.

The spectra (**Figure 5b**) obtained in the S 2p region before etching the negative electrode cycled in the [K,Cs][FSA] IL electrolyte displays only one broad peak assigned to the $–SO_2F$ species ($2p_{1/2}$ at 171.5 eV and $2p_{3/2}$ at 170.4 eV).[61] However, after Ar-ion etching, several peaks assigned to the $–SO_x–$ species emerge at 169.4 eV ($2p_{1/2}$ peak) and 167.8 eV ($2p_{3/2}$ peak).[62] The peaks observed around 163–164 eV were associated with –C–S– species[63], which evinces the possibility of a reaction between carbon from the graphite and $[FSA]^-$ decomposition product(s). Other peaks emerging near 160–161 eV were assigned to sulfide (S^{2-}) species.[61] The electrode further manifested some unknown peaks at binding energies below 160 eV, which could be attributed to some inorganic species.[61] Except for the peaks appearing below 160 eV in the case of [K,Cs][FSA], the S 2p XPS spectra from the two IL electrolyte operations show similar species before and after etching. Even so, the peak intensity of the sulfide (S^{2-}) species in the case of [K,Cs][FSA] is observed to be significantly higher than that from the $[K,C_3C_1pyrr][FSA]$ IL electrolyte. Drawing reference from a recent study pertaining to discrete fourier transform first principle calculations, the K^+ ion diffusion barrier (0.18 eV) in K_2S was found to be lower than that in KF (1.44 eV), which additionally affirms that the sulfide (S^{2-}) species in the electrode from the [K,Cs][FSA] IL aided in enhancing the K^+ ion diffusion.[64]

The spectra obtained in the F 1s region before etching the graphite electrode from both ILs (**Figure 5c** and **5f**) revealed the presence of –S–F species, denoted by the main peak and the shoulder peak appearing around 690.5 eV and 687 eV, respectively.[37] After Ar ion etching, the dominating peak was seen to shift to 684.4 eV, marking the formation of F^- species. Finally, the K 2p and Cs 3d XPS spectra obtained after Ar ion etching appear to be congruent with the K^+ and Cs^+ (most likely from KF and CsF), which are inorganic species (**Figure S5**).

To recapitulate the XPS results, the SEI layer formed on the graphite electrolyte by the [K,Cs][FSA] IL electrolyte is entirely comprised of inorganic species due to the absence of organic species in this electrolyte. Additionally, The higher amount of sulfide species (S^{2-}) present in the SEI layer of this electrolyte facilitates enhanced K^+ diffusion across the SEI layer. On the other hand, although the inner core of the SEI layer formed by the [K,C_3C_1pyrr][FSA] IL is mainly made of inorganic species (KF, –N=SO, –SO_x–, S^{2-}), the top layer encompasses (C–N^+) species, which are decomposition products from the [C_3C_1pyrr]$^+$ organic cation. The (C–N^+) is posited to exhibit poor charge transfer at the SEI layer, which can explain the poor performance visualized during operation with the organic IL electrolyte.

4. Conclusions

In this study, the physical and electrochemical behavior of the inorganic [K,Cs][FSA] IL electrolyte and the K^+ intercalation/deintercalation behavior of a graphite negative electrode during PIB operations are investigated in an effort to harness high rate capability and long cycle life from the negative electrode. Electrochemical tests on the graphite electrode (10 μm) in the present [K,Cs][FSA] IL electrolyte at 70 °C yielded a remarkable rate capability of 106 mAh g^{-1} at the current density of 100 C and high capacity retention of 98.7% after 450 cycles. Control analyses

conducted using the organic [K,C_3C_1pyrr][FSA] IL electrolyte at 70 °C demonstrated inferior rate capabilities, capacity fading accompanied by a peculiar increase in Coulombic efficiency (over 100%) after 150 cycles. The differences in the rate capabilities of the two IL electrolytes are entirely attributed to their interfacial resistance and inherently different SEI formation mechanisms. EIS measurements performed during cycling of the graphite/graphite symmetric cells demonstrated significantly lower interfacial resistance in the case of the [K,Cs][FSA] IL electrolyte as compared to the [K,C_3C_1pyrr][FSA] IL electrolyte. Through XPS analyses, the improvement in the performance of the [K,Cs][FSA] IL electrolyte is attributed to the inorganic compounds formed in the SEI layer after decomposition of the $[FSA]^-$during cycling. Further, the SEI formed by the [K,Cs][FSA] IL electrolyte is found to entail large amounts of sulfide species (S^{2-}) which are envisioned to enhance K^+ diffusion across the passivation layer. Herein, we demonstrate the use of high concentrations of K salts comprising the $[FSA]^-$ anion for intermediate-temperature PIB operations to be an expedient approach for harnessing high rate capabilities and long-term cycling performance from a large-particle size graphite electrode. Although the performance of the [K,C_3C_1pyrr][FSA] IL is still relatively high (compared with other PIB electrolytes) at intermediate temperature, its low K^+ ion concentration and the unstable SEI layer comprising inorganic compounds become significant drawbacks that limit its rate capability and cycle performance.

Acknowledgments

This work was supported by JSPS KAKENHI Grant Number 20K05144.

ASSOCIATED CONTENT

Supporting Information (PDF)

Supporting Information is available free of charge on the ACS Publications website at DOI: XXXXXXX.

Data for viscosity, ionic conductivity, vibrational spectroscopy, XRD, XPS, and electrochemical measurements.

AUTHOR INFORMATION

Corresponding Author

E-mail: k-matsumoto@energy.kyoto-u.ac.jp (K.M.).

Notes

The authors declare no competing financial interest.

ORCID

Shubham Kaushik: 0000-0002-2534-2897

Keigo Kubota: 0000-0002-0536-129X

Jinkwang Hwang: 0000-0003-4800-3158

Kazuhiko Matsumoto: 0000-0002-0770-9210

Rika Hagiwara: 0000-0002-7234-3980

Table 1. Electrochemical performance of a graphite negative electrode in select organic and ionic liquid electrolytes for PIBs

Graphite particle size/surface area (μm /m^2 g^{-1})	Mass loading (mg cm^{-2})	Electrolyte	Operating temperature (°C)	Binder /Graphite:binder wt % in electrode	Initial capacity/ Coulombic efficiency(mAh g^{-1}/ %)	Rate capability: Capacity (mAh g^{-1}) @ current density (mA g^{-1})	Cycle stability: Capacity retention (%) @ *n*th cycle / current density (mA g^{-1})	Ref.
3/-	0.8–1.0	1.0 mol dm^{-3} K[FSA] in EC:DEC	25	PANa/90:10	244/79	~230@4185 (potassiation at 27.9 mA g^{-1})	~100@50/25	[57]
3/-	~1.2	7.0 mol kg^{-1} K[FSA] in DME	25	PANa/90:10	260/80	~225@2790 (potassiation current = NA)	-	[19]
-/-	~8.0	6.91 mol kg^{-1} K[FSA] in DME	25	-	112/64.2	-	~116@300/25	[65]
-/-	~8.0	2.76 mol kg^{-1} K[FSA] in DME/HFE (1.90:0.95 in mol)	25	-	194/82.3	202@1255 (potassiation at 6.98 mA g^{-1})	103.1@300/25	[65]
-/7	~4.0	0.5 mol dm^{-3} K[PF_6] in DEGDME	25	PVDF/92:4 (AB = 4 wt%)	~110/90	56@279	74.6@50/25	[66]
-/7	~4.0	0.5 mol dm^{-3} K[PF_6] in EC:DEC	25	PVDF/92:4 (AB = 4 wt%)	~255/59	60@279	31.6@50/25	[66]
-/15	1.2–1.5	0.75 mol dm^{-3} K[PF_6] in EC:DEC	25	CMC/90:10	~239/74	226@4000 (potassiation at 20 mA g^{-1})	98.0@500/100	[67]
-/4	~2.0	1.0 mol dm^{-3} K[OTF] 2.0 in DEGDME	25	PVDF/90:10	105/62.9	78@10000	88.5@100/2000	[68]
3/-	-	K[FSA]-[C_3C_1pyrr][FSA] (2:8 in mol)	25	CMC/90:10	260/87	-	94.7@1000/558	[45]
-/-	1.5–2.0	K[FSA]-[C_3C_1pyrr][FSA] (2:8 in mol)	30	PAA/90:10	-/-	216@558	99@400/55.8	[44]
10/-	-	K[FSA]-K[FTA] (55:45 in mol)	80	PVDF/80:20	273/42.6	-	84.2@50/83.7	[46]
10/-	1.5	K[FSA]-Cs[FSA] (54:46 in mol)	70	PAI/80:20	278/66.0	106@27900	98.7@450/5580	This work

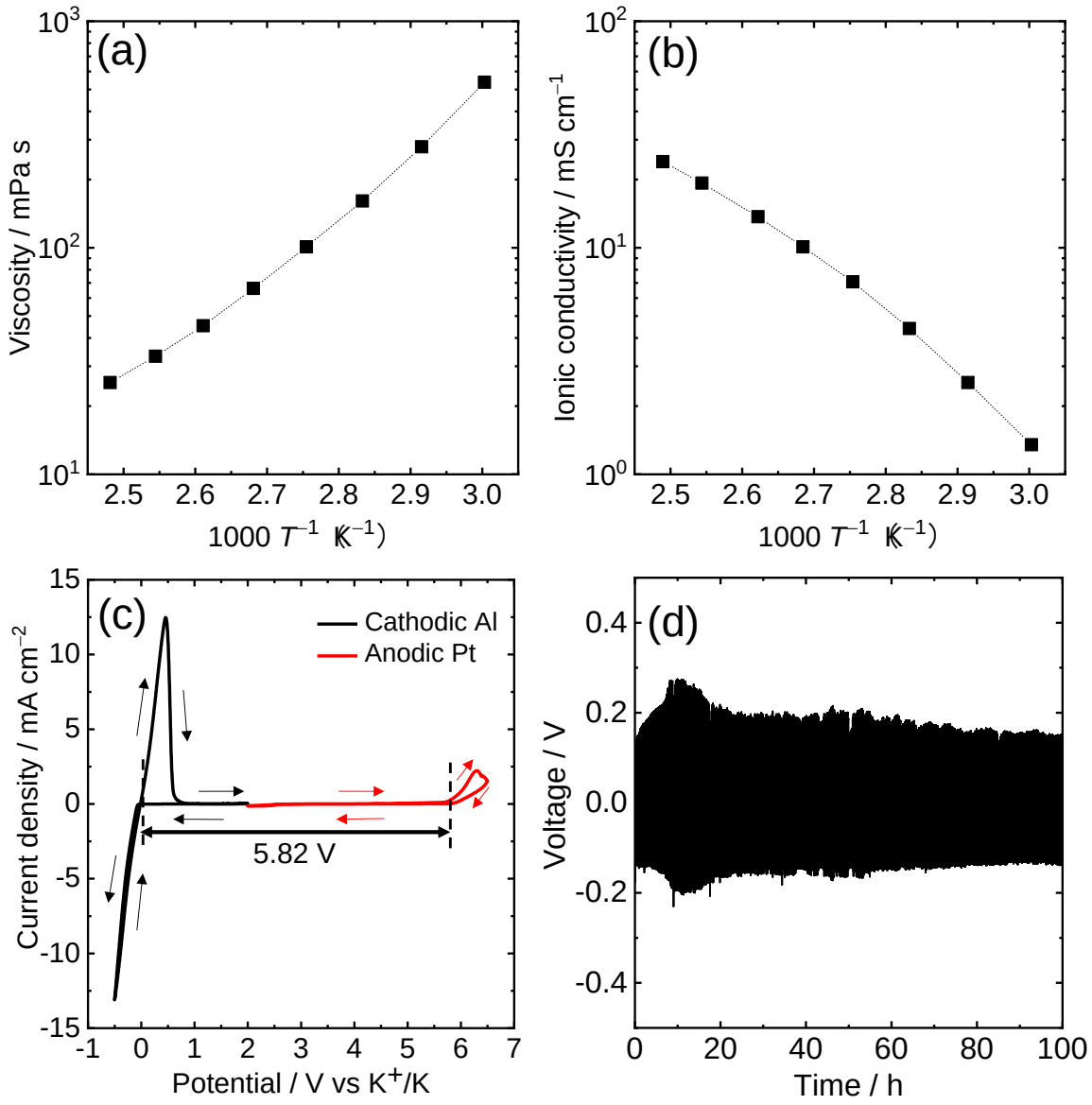

Figure 1. Temperature dependence of (a) viscosity and (b) ionic conductivity for the [K,Cs][FSA] IL electrolyte. (c) Combined cyclic voltammograms of Al (cathodic) and Pt (anodic) electrodes in the [K,Cs][FSA] IL electrolyte at a scan rate of 5 mV s^{-1} at 70 °C. [K,Cs][FSA] = K[FSA]-Cs[FSA] IL (54 : 46 in mol). (d) Deposition/dissolution test of K/K symmetric cells using [K, Cs][FSA] IL electrolyte at 70 °C for 100 h. Deposition and dissolution performed at 10 min per cycle (current density = 1 mA cm^{-2})

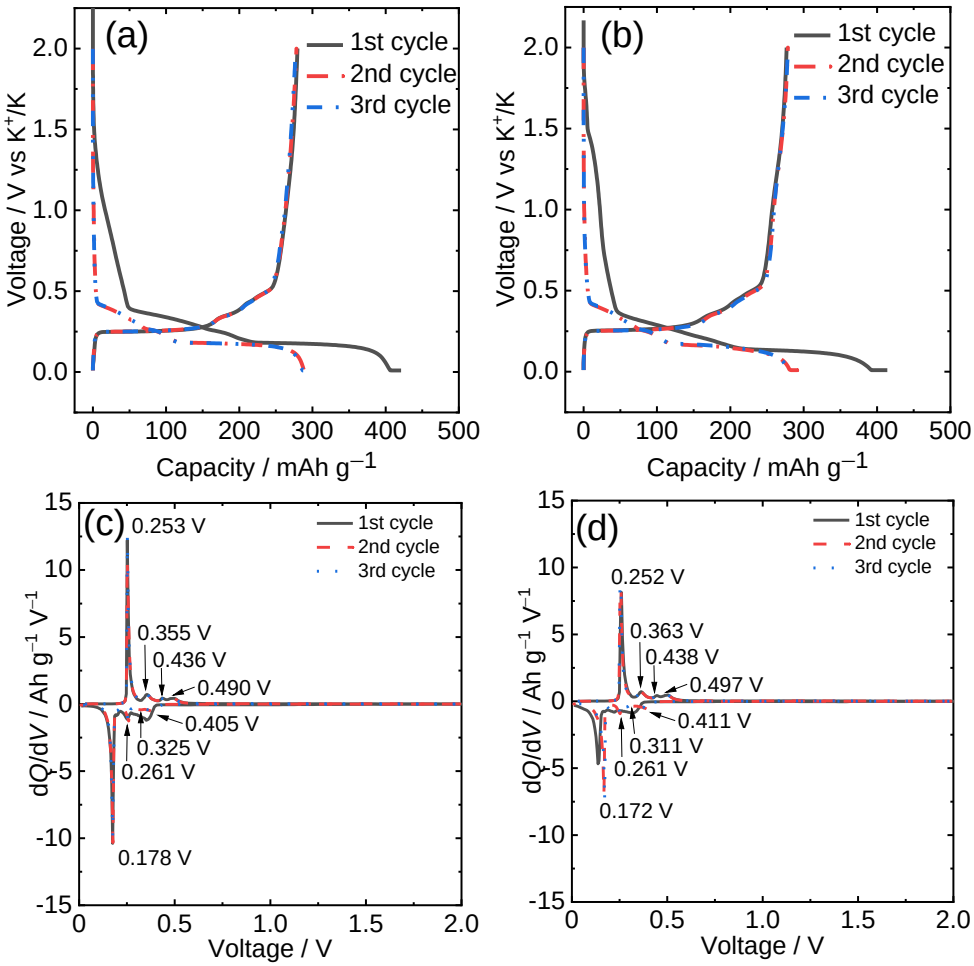

Figure 2. Electrochemical performance of K/graphite half-cells (graphite average particle size = 10 μm) at 70 °C in the 0.01–2.0 V cut-off voltage range. Charge-discharge curves of the cells with the (a) [K,Cs][FSA] IL and (b) [K,C_3C_1pyrr][FSA] IL electrolytes at a current density of 0.5C (additional constant voltage charging at 0.01 V). (c and d) The corresponding d*Q*/d*V* plots of the charge-discharge curves in (a and b). [K,Cs][FSA] = K[FSA]-Cs[FSA] IL (54 : 46 in mol) and [K,C_3C_1pyrr][FSA] = K[FSA]-[C_3C_1pyrr][FSA] IL (20 : 80 in mol).

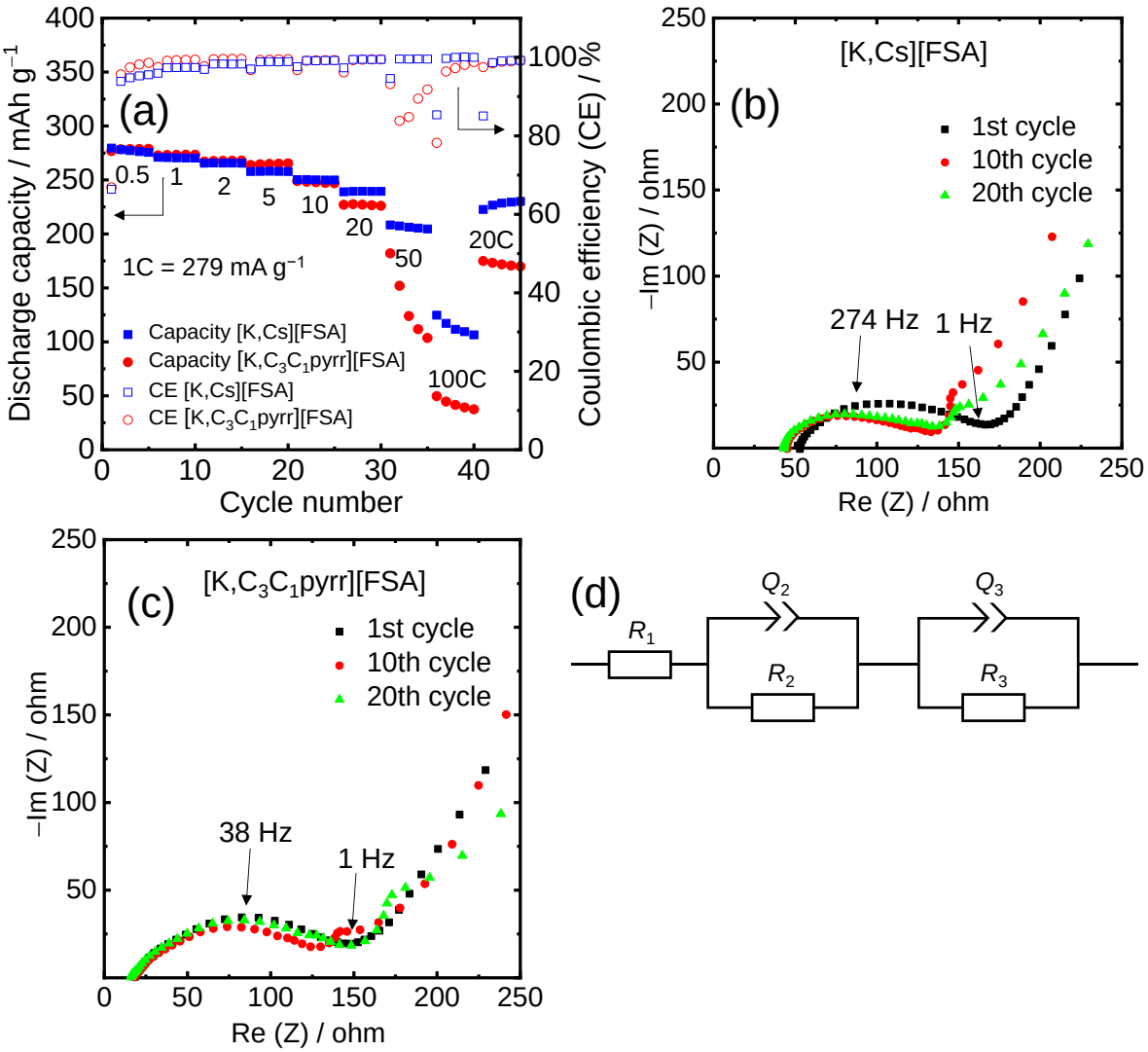

Figure 3. (a) Rate capability of K/graphite half-cells (graphite average particle size = 10 μm) employing the [K,Cs][FSA] IL and [K,C_3C_1pyrr][FSA] IL electrolytes. Current density = 0.5–100C (additional constant voltage charge at 0.01 V), cut-off voltage = 0.01–2.0 V. Nyquist plots of graphite/graphite symmetric-cells (electrode SOC = 50%) with the (b) [K,Cs][FSA] and (c) [K,C_3C_1pyrr][FSA] IL electrolytes at 1st, 10th, and 20th cycles. (d) Equivalent circuit used for fitting the Nyquist plots (see **Table S3** for the fitting parameters). [K,Cs][FSA] = K[FSA]-Cs[FSA] IL (54 : 46 in mol) and [K,C_3C_1pyrr][FSA] = K[FSA]-[C_3C_1pyrr][FSA] IL (20 : 80 in mol).

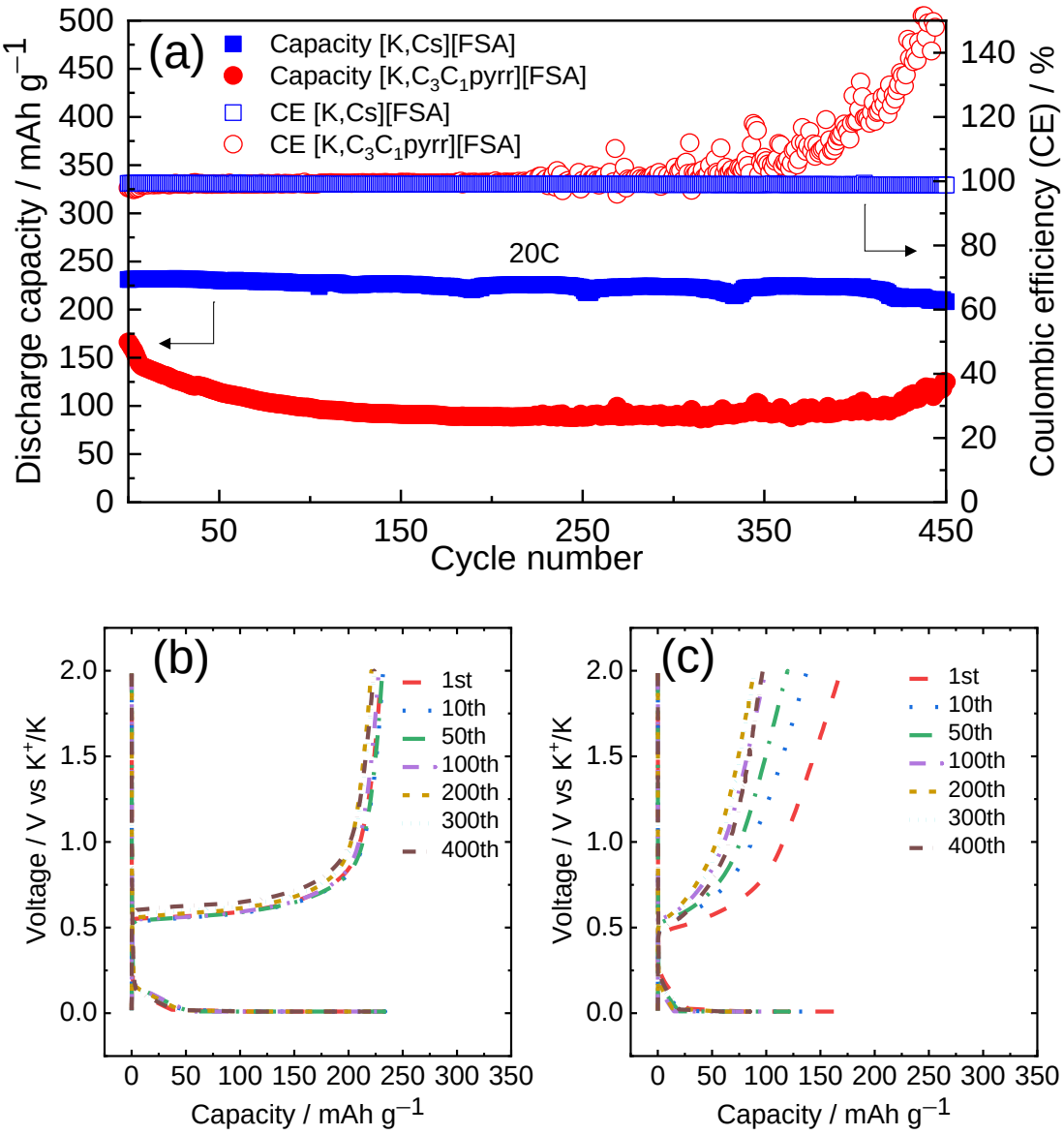

Figure 4. (**a**) Cycle performance of K/graphite half-cells (graphite average particle size = 10 µm) employing the [K,Cs][FSA] IL and [K,C_3C_1pyrr][FSA] IL electrolytes. Charge-discharge curves obtained during the cycle performance tests on cells with the (**b**) [K,Cs][FSA] IL and (**c**) [K,C_3C_1pyrr][FSA] IL electrolytes. Current density = 20C (additional constant voltage charge at 0.01 V), cut-off voltage = 0.01–2.0 V. [K,Cs][FSA] = K[FSA]-Cs[FSA] IL (54 : 46 in mol) and [K,C_3C_1pyrr][FSA] = K[FSA]-[C_3C_1pyrr][FSA] IL (20 : 80 in mol). The cycle tests presented here were performed after the rate capability tests.

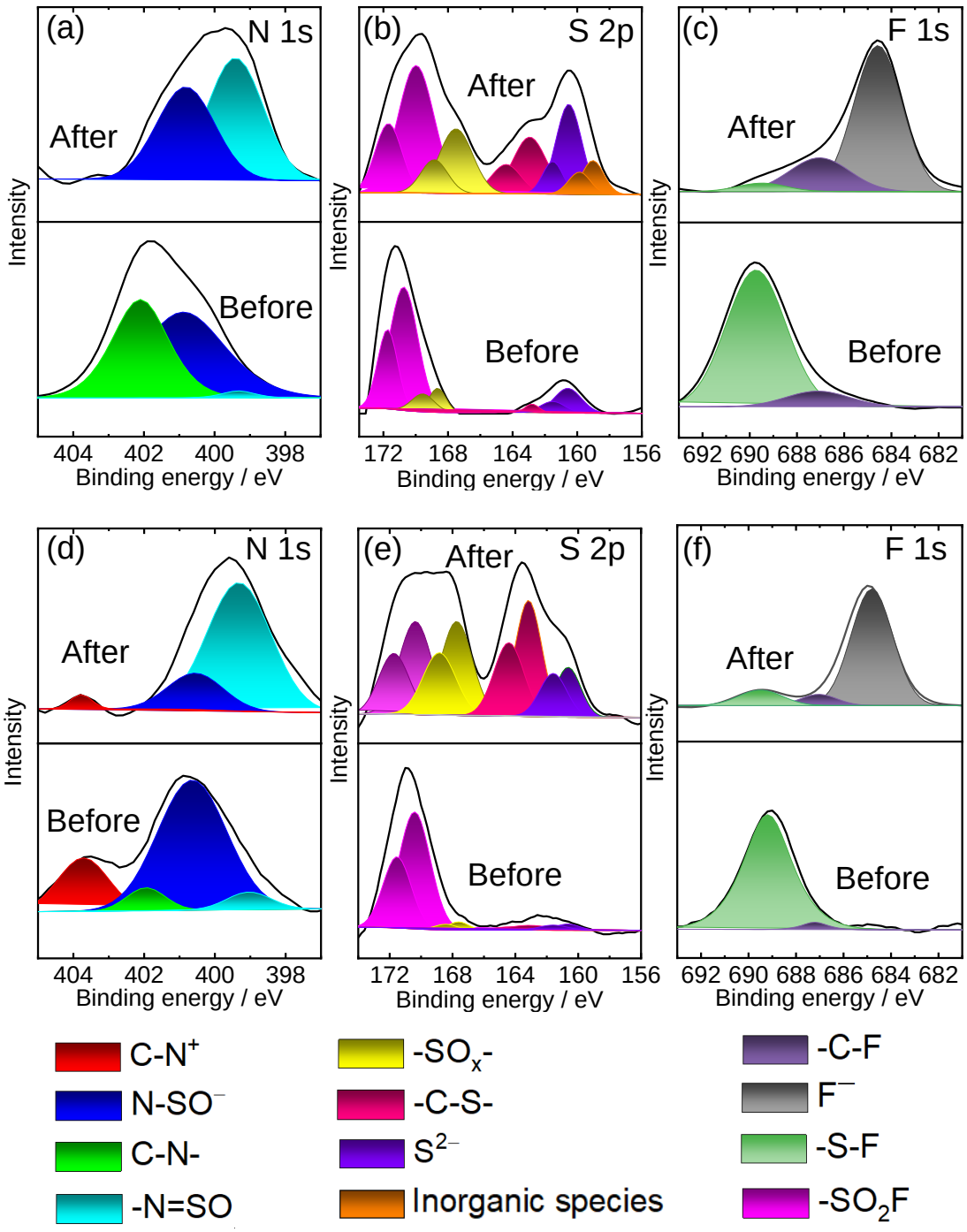

Figure 5. XPS spectra of the N 1s, S 2p, and F 1s regions of graphite negative electrodes obtained after one cycle in the (**a,b** and **c**) [K,Cs][FSA] IL and (**d,e** and **f**) [K,C_3C_1pyrr][FSA] IL electrolytes. The spectra were obtained before and after one-minute Ar ion etching. The peaks in the S 2p spectra appear as pairs because of the existence of $2p_{1/2}$ at a higher binding energy and $2p_{3/2}$ at a lower binding energy. (see **Figure 2** electrochemical data). [K,Cs][FSA] = K[FSA]-Cs[FSA] IL (54 : 46 in mol) and [K,C_3C_1pyrr][FSA] = K[FSA]-[C_3C_1pyrr][FSA] IL (20 : 80 in mol).

References

1. Scrosati, B.; Hassoun, J.; Sun, Y.-K., Lithium-Ion Batteries. A Look into the Future. *Energy Environ. Sci.* **2011,** *4*, 3287-3295.
2. Goodenough, J. B.; Park, K.-S., The Li-Ion Rechargeable Battery: A Perspective. *J. Am. Chem. Soc.* **2013,** *135*, 1167-1176.
3. Xu, J.; Dou, Y.; Wei, Z.; Ma, J.; Deng, Y.; Li, Y.; Liu, H.; Dou, S., Recent Progress in Graphite Intercalation Compounds for Rechargeable Metal (Li, Na, K, Al)-Ion Batteries. *Adv. Sci.* **2017,** *4*, 1700146.
4. Xie, J.; Zhang, Q., Recent Progress in Multivalent Metal (Mg, Zn, Ca, and Al) and Metal-Ion Rechargeable Batteries with Organic Materials as Promising Electrodes. *Small* **2019,** *15*, 1805061.
5. U.S. Geological Survey, Mineral Commodity Summaries, 2021. https://pubs.er.usgs.gov/publication/mcs2021 (accessed 6 March, 2022).
6. Ge, J.; Fan, L.; Rao, A. M.; Zhou, J.; Lu, B., Surface-Substituted Prussian Blue Analogue Cathode for Sustainable Potassium-Ion Batteries. *Nat. Sustain.* **2021**.
7. Ding, H.; Zhou, J.; Rao, A. M.; Lu, B., Cell-Like-Carbon-Micro-Spheres for Robust Potassium Anode. *Natl. Sci. Rev.* **2020,** *8*.
8. Okoshi, M.; Yamada, Y.; Komaba, S.; Yamada, A.; Nakai, H., Theoretical Analysis of Interactions between Potassium Ions and Organic Electrolyte Solvents: A Comparison with Lithium, Sodium, and Magnesium Ions. *J. Electrochem. Soc.* **2016,** *164*, A54-A60.
9. Zhang, X.; Meng, J.; Wang, X.; Xiao, Z.; Wu, P.; Mai, L., Comprehensive Insights into Electrolytes and Solid Electrolyte Interfaces in Potassium-Ion Batteries. *Energy Storage Mater.* **2021,** *38*, 30-49.
10. Pan, Q.; Gong, D.; Tang, Y., Recent Progress and Perspective on Electrolytes for Sodium/Potassium-Based Devices. *Energy Storage Mater.* **2020,** *31*, 328-343.
11. Pan, Q.; Tong, Z.; Su, Y.; Qin, S.; Tang, Y., Energy Storage Mechanism, Challenge and Design Strategies of Metal Sulfides for Rechargeable Sodium/Potassium-Ion Batteries. *Adv. Funct. Mater.* **2021,** *31*, 2103912.
12. Pan, Q.; Zheng, Y.; Tong, Z.; Shi, L.; Tang, Y., Novel Lamellar Tetrapotassium Pyromellitic Organic for Robust High-Capacity Potassium Storage. *Angew. Chem. Int. Ed.* **2021,** *60*, 11835-11840.
13. Wei, C.; Gong, D.; Xie, D.; Tang, Y. J. A. E. L., The Free-Standing Alloy Strategy to Improve the Electrochemical Performance of Potassium-Based Dual-Ion Batteries. *ACS Energy Lett.* **2021,** *6*, 4336-4344.
14. Zhang, E.; Jia, X.; Wang, B.; Wang, J.; Yu, X.; Lu, B., Carbon Dots@rGO Paper as Freestanding and Flexible Potassium-Ion Batteries Anode. *Adv. Mater.* **2020,** *7*, 2000470.
15. Ge, J.; Wang, B.; Zhou, J.; Liang, S.; Rao, A. M.; Lu, B., Hierarchically Structured Nitrogen-Doped Carbon Microspheres for Advanced Potassium Ion Batteries. *ACS Mater. Lett.* **2020,** *2*, 853-860.
16. Jian, Z.; Luo, W.; Ji, X., Carbon Electrodes for K-Ion Batteries. *J. Am. Chem. Soc.* **2015,** *137*, 11566-11569.
17. Fan, L.; Chen, S.; Ma, R.; Wang, J.; Wang, L.; Zhang, Q.; Zhang, E.; Liu, Z.; Lu, B., Ultrastable Potassium Storage Performance Realized by Highly Effective Solid Electrolyte Interphase Layer. *Small* **2018,** *14*, 1801806.

18. Hosaka, T.; Matsuyama, T.; Kubota, K.; Yasuno, S.; Komaba, S., Development of Kpf6/Kfsa Binary-Salt Solutions for Long-Life and High-Voltage K-Ion Batteries. *ACS Appl. Mater. Interfaces* **2020,** *12*, 34873-34881.
19. Hosaka, T.; Kubota, K.; Kojima, H.; Komaba, S., Highly Concentrated Electrolyte Solutions for 4 V Class Potassium-Ion Batteries. *Chem. Commun.* **2018,** *54*, 8387-8390.
20. Xiao, N.; McCulloch, W. D.; Wu, Y., Reversible Dendrite-Free Potassium Plating and Stripping Electrochemistry for Potassium Secondary Batteries. *J. Am. Chem. Soc.* **2017,** *139*, 9475-9478.
21. Liu, S.; Mao, J.; Zhang, Q.; Wang, Z.; Pang, W. K.; Zhang, L.; Du, A.; Sencadas, V.; Zhang, W.; Guo, Z., An Intrinsically Non-Flammable Electrolyte for High-Performance Potassium Batteries. *Angew. Chem. Int. Ed.* **2020,** *59*, 3638-3644.
22. Hess, M., Non-Linearity of the Solid-Electrolyte-Interphase Overpotential. *Electrochim. Acta* **2017,** *244*, 69-76.
23. Armand, M.; Endres, F.; MacFarlane, D. R.; Ohno, H.; Scrosati, B., Ionic-Liquid Materials for the Electrochemical Challenges of the Future. *Nat. Mater.* **2009,** *8*, 621-629.
24. Matsumoto, K.; Hwang, J.; Kaushik, S.; Chen, C.-Y.; Hagiwara, R., Advances in Sodium Secondary Batteries Utilizing Ionic Liquid Electrolytes. *Energy Environ. Sci.* **2019,** *12*, 3247-3287.
25. Xiong, S.; Xie, K.; Blomberg, E.; Jacobsson, P.; Matic, A., Analysis of the Solid Electrolyte Interphase Formed with an Ionic Liquid Electrolyte for Lithium-Sulfur Batteries. *J. Power Sources* **2014,** *252*, 150-155.
26. Wang, D.; Hwang, J.; Chen, C.-y.; Kubota, K.; Matsumoto, K.; Hagiwara, R., A B"-Alumina/Inorganic Ionic Liquid Dual Electrolyte for Intermediate-Temperature Sodium–Sulfur Batteries. *Adv. Funct. Mater.* **2021**, *31*, 2105524.
27. Watanabe, M.; Thomas, M. L.; Zhang, S.; Ueno, K.; Yasuda, T.; Dokko, K., Application of Ionic Liquids to Energy Storage and Conversion Materials and Devices. *Chem. Rev.* **2017,** *117*, 7190-7239.
28. MacFarlane, D. R.; Tachikawa, N.; Forsyth, M.; Pringle, J. M.; Howlett, P. C.; Elliott, G. D.; Davis, J. H.; Watanabe, M.; Simon, P.; Angell, C. A., Energy Applications of Ionic Liquids. *Energy Environ. Sci.* **2014,** *7*, 232-250.
29. Ohno, H., *Electrochemical Aspects of Ionic Liquids*. John Wiley & Sons: 2005; p 392.
30. Fukunaga, A.; Nohira, T.; Hagiwara, R.; Numata, K.; Itani, E.; Sakai, S.; Nitta, K.; Inazawa, S., A Safe and High-Rate Negative Electrode for Sodium-Ion Batteries: Hard Carbon in Nafsa-C1c3pyrfsa Ionic Liquid at 363 k. *J. Power Sources* **2014,** *246*, 387-391.
31. Chen, C.-Y.; Kiko, T.; Hosokawa, T.; Matsumoto, K.; Nohira, T.; Hagiwara, R., Ionic Liquid Electrolytes with High Sodium Ion Fraction for High-Rate and Long-Life Sodium Secondary Batteries. *J. Power Sources* **2016,** *332*, 51-59.
32. Hagiwara, R.; Matsumoto, K.; Hwang, J.; Nohira, T., Sodium Ion Batteries Using Ionic Liquids as Electrolytes. *Chem. Rec.* **2019,** *19*, 758-770.
33. Lin, X.; Salari, M.; Arava, L. M. R.; Ajayan, P. M.; Grinstaff, M. W., High Temperature Electrical Energy Storage: Advances, Challenges, and Frontiers. *Chem. Soc. Rev.* **2016,** *45*, 5848-5887.
34. Dahbi, M.; Fukunishi, M.; Horiba, T.; Yabuuchi, N.; Yasuno, S.; Komaba, S., High Performance Red Phosphorus Electrode in Ionic Liquid-Based Electrolyte for Na-Ion Batteries. *J. Power Sources* **2017,** *363*, 404-412.
35. Arano, K.; Begic, S.; Chen, F.; Rakov, D.; Mazouzi, D.; Gautier, N.; Kerr, R.; Lestriez, B.; Le Bideau, J.; Howlett, P. C., Tuning the Formation and Structure of the Silicon Electrode/Ionic

Liquid Electrolyte Interphase in Superconcentrated Ionic Liquids. *ACS Appl. Mater. Interfaces* **2021**.
36. Hwang, J.; Okada, H.; Haraguchi, R.; Tawa, S.; Matsumoto, K.; Hagiwara, R., Ionic Liquid Electrolyte for Room to Intermediate Temperature Operating Li Metal Batteries: Dendrite Suppression and Improved Performance. *J. Power Sources* **2020,** *453*, 227911.
37. Sun, J.; O'Dell, L. A.; Armand, M.; Howlett, P. C.; Forsyth, M., Anion-Derived Solid-Electrolyte Interphase Enables Long Life Na-Ion Batteries Using Superconcentrated Ionic Liquid Electrolytes. *ACS Energy Lett.* **2021,** *6*, 2481-2490.
38. Yamamoto, T.; Matsumoto, K.; Hagiwara, R.; Nohira, T., Physicochemical and Electrochemical Properties of K[N(SO2F)2]–[N-Methyl-N-Propylpyrrolidinium][N(SO2F)2] Ionic Liquids for Potassium-Ion Batteries. *J. Phys. Chem. C* **2017,** *121*, 18450-18458.
39. Masese, T.; Yoshii, K.; Kato, M.; Kubota, K.; Huang, Z.-D.; Senoh, H.; Shikano, M., A High Voltage Honeycomb Layered Cathode Framework for Rechargeable Potassium-Ion Battery: P2-Type K2/3Ni1/3Co1/3Te1/3O2. *Chem. Commun.* **2019,** *55*, 985-988.
40. Masese, T.; Yoshii, K.; Yamaguchi, Y.; Okumura, T.; Huang, Z.-D.; Kato, M.; Kubota, K.; Furutani, J.; Orikasa, Y.; Senoh, H.; Sakaebe, H.; Shikano, M., Rechargeable Potassium-Ion Batteries with Honeycomb-Layered Tellurates as High Voltage Cathodes and Fast Potassium-Ion Conductors. *Nat. Commun.* **2018,** *9*, 3823.
41. Arnaiz, M.; Bothe, A.; Dsoke, S.; Balducci, A.; Ajuria, J., Aprotic and Protic Ionic Liquids Combined with Olive Pits Derived Hard Carbon for Potassium-Ion Batteries. *J. Electrochem. Soc.* **2019,** *166*, A3504-A3510.
42. Yamamoto, T.; Nohira, T., Tin Negative Electrodes Using an FSA-Based Ionic Liquid Electrolyte: Improved Performance of Potassium Secondary Batteries. *Chem. Commun.* **2020,** *56*, 2538-2541.
43. Domi, Y.; Usui, H.; Nakabayashi, E.; Yamamoto, T.; Nohira, T.; Sakaguchi, H., Potassiation and Depotassioation Properties of Sn4P3 Electrode in an Ionic-Liquid Electrolyte. *Electrochemistry* **2019,** *87*, 333-335.
44. Fiore, M.; Wheeler, S.; Hurlbutt, K.; Capone, I.; Fawdon, J.; Ruffo, R.; Pasta, M., Paving the Way toward Highly Efficient, High-Energy Potassium-Ion Batteries with Ionic Liquid Electrolytes. *Chem. Mater.* **2020,** *32*, 7653-7661.
45. Onuma, H.; Kubota, K.; Muratsubaki, S.; Hosaka, T.; Tatara, R.; Yamamoto, T.; Matsumoto, K.; Nohira, T.; Hagiwara, R.; Oji, H.; Yasuno, S.; Komaba, S., Application of Ionic Liquid as K-Ion Electrolyte of Graphite//K2Mn[Fe(CN)6] Cell. *ACS Energy Lett.* **2020,** *5*, 2849-2857.
46. Yamamoto, H.; Chen, C.-Y.; Kubota, K.; Matsumoto, K.; Hagiwara, R., Potassium Single Cation Ionic Liquid Electrolyte for Potassium-Ion Batteries. *J. Phys. Chem. B* **2020,** *124*, 6341-6347.
47. Xu, W.; Wang, H.; Hu, J.; Zhang, H.; Zhang, B.; Kang, F.; Zhai, D., A Highly Concentrated Electrolyte for High-Efficiency Potassium Metal Batteries. *Chem. Commun.* **2021,** *57*, 1034-1037.
48. Kubota, K.; Nohira, T.; Hagiwara, R., Thermal Properties of Alkali Bis(Fluorosulfonyl)Amides and Their Binary Mixtures. *J. Chem. Eng. Data* **2010,** *55*, 3142-3146.
49. Kubota, K.; Nohira, T.; Hagiwara, R., New Inorganic Ionic Liquids Possessing Low Melting Temperatures and Wide Electrochemical Windows: Ternary Mixtures of Alkali Bis(Fluorosulfonyl)Amides. *Electrochim. Acta* **2012,** *66*, 320-324.
50. Matsumoto, K.; Oka, T.; Nohira, T.; Hagiwara, R., Polymorphism of Alkali Bis(Fluorosulfonyl)Amides (M[N(SO2F)2], M = Na, K, and Cs). *Inorg. Chem.* **2013,** *52*, 568-576.

51. Vogel, H., The Temperature Dependence Law of the Viscosity of Fluids. *Phys. Z* **1921,** *22*, 645-646.
52. Tokuda, H.; Hayamizu, K.; Ishii, K.; Susan, M. A. B. H.; Watanabe, M., Physicochemical Properties and Structures of Room Temperature Ionic Liquids. 1. Variation of Anionic Species. *J. Phys. Chem. B* **2004,** *108*, 16593-16600.
53. MacFarlane, D. R.; Forsyth, M.; Izgorodina, E. I.; Abbott, A. P.; Annat, G.; Fraser, K., On the Concept of Ionicity in Ionic Liquids. *Phys. Chem. Chem. Phys.* **2009,** *11*, 4962-4967.
54. Carboni, M.; Naylor, A. J.; Valvo, M.; Younesi, R., Unlocking High Capacities of Graphite Anodes for Potassium-Ion Batteries. *RSC Adv.* **2019,** *9*, 21070-21074.
55. Dresselhaus, M. S.; Dresselhaus, G., Intercalation Compounds of Graphite. *Adv. phys.* **2002,** *51*, 1-186.
56. Zhao, J.; Zou, X.; Zhu, Y.; Xu, Y.; Wang, C., Electrochemical Intercalation of Potassium into Graphite. *Adv. Funct. Mater.* **2016,** *26*, 8103-8110.
57. Komaba, S.; Hasegawa, T.; Dahbi, M.; Kubota, K., Potassium Intercalation into Graphite to Realize High-Voltage/High-Power Potassium-Ion Batteries and Potassium-Ion Capacitors. *Electrochem. Commun.* **2015,** *60*, 172-175.
58. Liu, S.; Ji, X.; Piao, N.; Chen, J.; Eidson, N.; Xu, J.; Wang, P.; Chen, L.; Zhang, J.; Deng, T.; Hou, S.; Jin, T.; Wan, H.; Li, J.; Tu, J.; Wang, C., An Inorganic-Rich Solid Electrolyte Interphase for Advanced Lithium-Metal Batteries in Carbonate Electrolytes. *Angew. Chem. Int. Ed.* **2021,** *60*, 3661-3671.
59. Kamphaus, E. P.; Angarita-Gomez, S.; Qin, X.; Shao, M.; Engelhard, M.; Mueller, K. T.; Murugesan, V.; Balbuena, P. B., Role of Inorganic Surface Layer on Solid Electrolyte Interphase Evolution at Li-Metal Anodes. *ACS Appl. Mater. Interfaces* **2019,** *11*, 31467-31476.
60. Xu, M.; Li, Y.; Ihsan-Ul-Haq, M.; Mubarak, N.; Liu, Z.; Wu, J.; Luo, Z.; Kim, J. K., Naf-Rich Solid Electrolyte Interphase for Dendrite-Free Sodium Metal Batteries. *Energy Storage Mater.* **2022,** *44*, 477-486.
61. Yu, X.-R.; Liu, F.; Wang, Z.-Y.; Chen, Y., Auger Parameters for Sulfur-Containing Compounds Using a Mixed Aluminum-Silver Excitation Source. *J. Electron. Spectrosc. Relat. Phenom.* **1990,** *50*, 159-166.
62. Contarini, S.; Rabalais, J. W., Ion Bombardment-Induced Decomposition of Li and Ba Sulfates and Carbonates Studied by X-Ray Photoelectron Spectroscopy. *J. Electron. Spectrosc. Relat. Phenom.* **1985,** *35*, 191-201.
63. Lindberg, B. J.; Hamrin, K.; Johansson, G.; Gelius, U.; Fahlman, A.; Nordling, C.; Siegbahn, K., Molecular Spectroscopy by Means of Esca Ii.Sulfur Compounds. Correlation of Electron Binding Energy with Structure. *Phys. Scr.* **1970,** *1*, 286-298.
64. Park, J.; Jeong, Y.; Alfaruqi, M. H.; Liu, Y.; Xu, X.; Xiong, S.; Jung, M.-G.; Jung, H.-G.; Kim, J.; Hwang, J.-Y.; Sun, Y.-K., Stable Solid Electrolyte Interphase for Long-Life Potassium Metal Batteries. *ACS Energy Lett.* **2021**, 401-409.
65. Qin, L.; Xiao, N.; Zheng, J.; Lei, Y.; Zhai, D.; Wu, Y., Localized High-Concentration Electrolytes Boost Potassium Storage in High-Loading Graphite. *Adv. Energy Mater.* **2019,** *9*, 1902618.
66. Lei, Y.; Han, D.; Dong, J.; Qin, L.; Li, X.; Zhai, D.; Li, B.; Wu, Y.; Kang, F., Unveiling the Influence of Electrode/Electrolyte Interface on the Capacity Fading for Typical Graphite-Based Potassium-Ion Batteries. *Energy Storage Mater.* **2020,** *24*, 319-328.
67. Rahman, M. M.; Hou, C.; Mateti, S.; Tanwar, K.; Sultana, I.; Glushenkov, A. M.; Chen, Y., Documenting Capacity and Cyclic Stability Enhancements in Synthetic Graphite Potassium-

Ion Battery Anode Material Modified by Low-Energy Liquid Phase Ball Milling. *J. Power Sources* **2020,** *476*, 228733.
68. Li, L.; Liu, L.; Hu, Z.; Lu, Y.; Liu, Q.; Jin, S.; Zhang, Q.; Zhao, S.; Chou, S.-L., Understanding High-Rate K+-Solvent Co-Intercalation in Natural Graphite for Potassium-Ion Batteries. *Angew. Chem. Int. Ed.* **2020,** *59*, 12917-12924.

For Table of Contents Only